LUND UNIVERSITY
Faculty of Science

DEPARTMENT OF PHYSICS
AND
SP TECHNICAL RESEARCH INSTITUTE OF SWEDEN

BACHELOR THESIS

Characterization of a Zeeman Slower Designed for a ^{87}Sr Optical Clock

Author:
Jonas OLSSON

Supervisors:
Martin ZELAN
Mathieu GISSELBRECHT

Abstract

Optical clocks will potentially become the new frequency standard for the SI-definition of the second. Many national metrology institutes around the world have already implemented different versions of such clocks and others are in process of doing so. At SP Technical Research Institute of Sweden, this process has recently begun. This thesis investigates the properties of the Zeeman slower that is to be used as part of the clock. A simple Gaussmeter was constructed from a semiconductor Hall sensor and used to measure the magnetic field profile of the slower. This report also contains the design for an electronic control circuit based on the Arduino platform, which can be used to control the magnetic field. The results showed that the particular slower investigated here will likely not need a control circuit. However, the control circuit can be used in other optical clocks or even in other applications.

January 9, 2015

Acknowledegments

This project has been a great learning opportunity for me. I have learned quite a bit about both laser physics and electronics design. I would like to thank my supervisor Martin Zelan, not only for patiently (mostly) sharing his knowledge of laser physics, but also for his hospitality during my stay in Borås. Thanks also go out to Sven-Christian Ebenhag for providing me with relevant information and insights into electronics design. Per Olof Hedekvist and Oscar Mollmyr also deserve thanks for helping me with certain parts of the circuit design.

Contents

1 Introduction

1.1 Motivation

Over the course of history there have been many different systems from which different physical quantities have been defined. The most prevalent system in use today in the scientific and engineering communities is the metric system and in particular *Système International d'Unités*, the SI-system. The system is regulated by the organization Bureau international des poids et mesures (BIPM) in France. A quantity like mass has the standard unit kilogram in this system, and BIPM maintain the internationl prototypes that define the kilogram. Other organizations can then opt to use this system and calibrate their standards against the BIPM definitions. One such organization is a national metrology institute (NMI). SP Technical Research Institute of Sweden (SP) is the NMI in Sweden and is hence appointed by the government to fulfill the responsibility of maintaining the units in the SI-system. This allows research and business interests in Sweden to calibrate their eqipment against the standards at SP. One important aspect of this process is that all standards and calibrations are traceable back to the prototypes at BIPM.

The unit of interest in this thesis is the second. The second is defined in terms of a frequency standard; the number of oscillations in an electromagnetic wave. It is defined at the time of writing as: *'the duration of 9192631770 periods of the radiation corresponding to the transition between the two hyperfine levels of the ground state of the cesium 133 atom'* [1]. It was accepted in 1967 and reflected the technological advances made in atomic physics during the 40s and 50s.

Over the past thirty years similar technological advances have been made which potentially can improve the current frequency standard. The new methods are based on different atoms that produce higher, optical frequencies, so called optical atomic clocks. SP is currently looking into building a clock based on neutral ^{87}Sr atoms. This thesis work is concerned with the study of such a clock.

1.2 Principles of an atomic clock

1.2.1 How to measure time

A clock is the basis of measuring time. In its simplest form, a clock is a periodic phenomenon combined with a device that counts each time the period repeats from a given starting point. This is usually called the oscillator and the counter. This simple arrangement divides time into smaller pieces, each with a length corresponding to the period of the oscillator. By increasing the frequency of the oscillator it is possible to subdivide time even further.

1.2.2 Atomic clocks

A time standard based on atomic transitions has two main advantages. Firstly, the microwave transition in cesium provides a high frequency oscillator which leads to high accuracy. Secondly, the atomic transition is stable over time which makes it ideal as a reference.

Furthermore, since the transition frequency is in the microwave range it can readily be measured with regular electronics. Many technologies where high-speed synchronization is required, such as GPS navigation, are now reliant on atomic clocks to function [2]. Because of atomic clocks the second is the most accurate unit of measurement and many other units are partially derived in terms of the second [2].

However, there are some limitations to the precision of the atomic cesium clock. This is mainly related to the temperature of the atoms in these clocks. The atoms have a relatively high temperature which causes the interaction time of the atoms with the microwave cavity to be short. This limits the number of atoms that can be excited. The velocity also introduces Doppler and collision effects into the system, which limits the accuracy. However, the problem could be removed almost completely if the atoms could be cooled to very low temperatures.

1.2.3 Laser cooling

Research into laser cooling started in the 1970s and the field now contains many different techniques to cool atoms to very low temperatures. These techniques are so efficient that it is possible to cool atoms from $\sim 1000\,\mathrm{K}$ down to below $\sim 1\,\mu\mathrm{K}$ [3].

A modern laser cooling experiment will typically consist of different stages designed to cool atoms to a point where they can be trapped for further measurements. The first stage is typically a heating mechanism, such as an atomic oven. This evaporates the atoms into a gas which is then collimated into a beam. After creating the beam, the atoms need to be slowed down again. The first part in doing so is typically the Zeeman slower [4], although other methods are available. The idea behind it is to use a laser which, when tuned correctly to account for the Doppler shift, exerts a scattering force on the atoms. This is covered further in the section 1.3.2.

The next step is to trap the atoms in what is called a *magneto optical trap* (MOT) [5] [6] [7]. This technique is based on a sealed, vacuum chamber with three detuned and orthogonal lasers that slow the atomic motion in all directions. The lasers are combined with an anti-helmholtz magnetic field to keep the atoms trapped in the center [3]. In a similar way to how the Zeeman slower operates, the MOT uses the magnetic fields to create an increasing Zeeman shift as the atoms move off-center. The shifted energy level allows the lasers to be on resonance with the atomic transition again and keeps the atoms contained in a small volume. This basic three-stage setup is illustrated in figure 1.

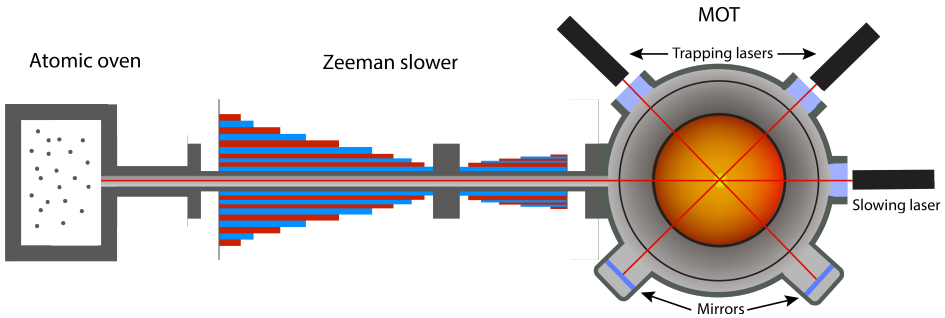

Figure 1: A side view and cross section of a typical laser cooling experiment. The atoms are heated in the oven and the slowing process begins in the Zeeman slower. Once the atoms reach the MOT their thermal velocity is low enough to trap them with three orthogonal and mirrored lasers. Only two of the lasers are shown, the third is aligned into or out of the page. The trapped and glowing atomic cloud is illustrated in the center of the MOT.

There have been further improvements made to the MOT, like optical lattice trapping.

This technique uses interfering lasers to create a standing wave. This wave act as an optical lattice potential, similar to the lattice potential in a solid. If the atoms have a low enough thermal energy they can be caught in this potential [3].

Laser cooling has also allowed new research into Bose-Einstein condensates [8] [9]. By trapping atoms in either a magnetic or optical potential it is possible to cool atoms even further and create a condensate. The technique is called evaporative cooling and the mechanism is similar to how a hot liquid cools off. By continuously lowering the trapping potential the more energetic particles will escape. Eventually the condensate will form as all the atoms are forced into the ground state.

1.2.4 Optical atomic clocks

There has been much interest in using other atomic species and transitions to create higher optical frequencies and improve clock accuracy. Microwave frequency clocks are limited by their frequency, but the system as a whole can run for longer periods. This leads to improved accuracy and stability over time because statistical effects can be minimized by averaging the data. The best cesium fountain clocks today are able to reach a relative uncertainty of $\sim 10^{-16}$ [2]. The optical clocks in use today have a higher short-term accuracy but they are difficult to operate over time.

There are two main types of optical clocks: the ion clock and the lattice clock. The ion clock is based on transitions in a single magnetically trapped ion [10]. The lattice clock on the other hand is based on manipulation of a large number of neutral atoms trapped in an optical lattice potential [11]. A comparison of a few different clocks are shown in figure 2.

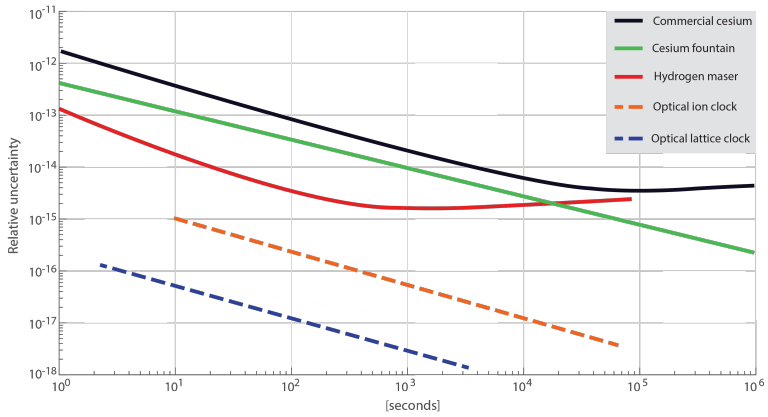

Figure 2: Schematic Allan variance plot. The Allan variance is a statistical tool developed to take into account the often noisy signal in oscillators [12]. The plot is a log-log plot which shows how the uncertainty (variance) in the time measurement varies over time. The commercial cesium and hydrogen maser clocks improve up to a point, after which environmental factors like temperature start to negatively affect the stability. The optical ion and lattice clocks reach higher accuracy in a short time but can be improved further if the operation could be stabilized.

An optical clock is a clock that uses optical frequency transitions instead of microwave transitions. Optical wavelengths are in the range 380 nm - 750 nm [13], which corresponds

to frequencies between $\sim 4 \cdot 10^{14}$ Hz - $7.9 \cdot 10^{14}$ Hz. Compared to the microwave transition in cesium, the improvement is almost five orders of magnitude. This is the main reason why optical clocks will likely become the new standard for accurate time measurements. However, to realize an optical frequency standard creates a technical measurement problem; most electronic equipment cannot register such fast oscillations.

This was solved with the advent of the femtosecond frequency comb [4]. Modern frequency combs use ultra-stable mode-locked lasers with a pulse width $t_{\mathrm{w}} \sim 10^{-15}$s to create very short pulses. Depending on the laser resonator length the repetition time t_{rep} of these pulses range between $1\,\mathrm{ns} \lesssim t_{\mathrm{rep}} \lesssim 100\,\mathrm{ns}$, or equivalently, a repetition frequency $f_{\mathrm{rep}} = 1/t_{\mathrm{rep}}$ between $10\,\mathrm{MHz} \lesssim f_{\mathrm{rep}} \lesssim 1\,\mathrm{GHz}$ [14]. The frequency domain spectrum of the signal looks like a 'comb' of discrete frequencies separated by f_{rep}. The femtosecond pulse width is enough to create a frequency spectrum spanning a complete octave, and can cover the entire optical frequency range [14], see figure 3. The frequency range in an ideal frequency comb can be expressed as [3]

$$f(n) = f_0 + nf_{rep}, \tag{1}$$

where f_0 is the offset from zero and n denotes the n:th 'comb tooth' in the range.

The comb can be used as a frequency reference and works as a 'translator' between optical and radio- or microwave frequencies. By mixing an unknown frequency of interest, for instance an optical signal, with the comb signal will create a beat frequency. The beat frequency will be in the radio- or microwave range, which is much lower than the clock frequency and can readily be measured with electronic counters.

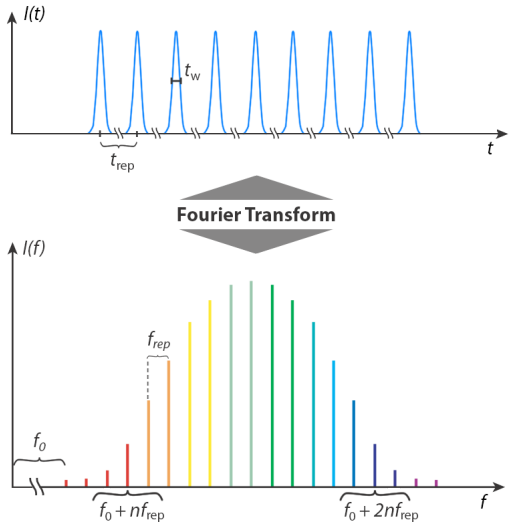

Figure 3: Simplified and conceptual figure over the frequency comb. The above image shows the femtosecond laser pulses in the time domain. The time between each pulse is t_{rep} and the pulse width is t_{w}, where $t_{\mathrm{rep}} \gg t_{\mathrm{w}}$. Only a few of the available frequencies are shown here, in reality $n \sim 10^6$. The figure is adapted from [14].

1.3 Principles of a Zeeman slower

The Zeeman slower is the main focus of this thesis and in particular the magnetic field profile. This section will cover some concepts in order to explain the Zeeman slower. Firstly, the theory of Doppler broadening will be covered. Secondly, the most basic process of laser cooling will be introduced. Lastly, the Zeeman slower is explained and it is shown how it can be used to cool atoms to low temperatures.

1.3.1 Doppler broadening

If an atom in a gas is travelling at some velocity **v** when it absorbs or emits a photon, then the observed frequency of the photon will be higher or lower with regards to the actual atomic transition. This is the Doppler effect and can be stated as

$$\omega = \omega_0 + \mathbf{kv}, \tag{2}$$

where ω is the angular frequency in the lab frame and ω_0 is the resonance frequency of the atom in its rest frame. The term **kv** gives the Doppler shift as the product of the atomic velocity and the wavevector of the radiation. Depending on the relative direction of these vectors, the absorbed or emitted radiation frequency will increase or decrease.

Furthermore, the atoms in the gas do not have a uniform velocity. However, is possible to describe the atomic velocities in a beam with the most probable velocity u. This is given by

$$u = \sqrt{\frac{3k_{\mathrm{B}}T}{M}}, \tag{3}$$

where k_{B} is Boltzmann's constant, T is the temperature and M is the atomic mass. The velocity distribution and equation 3 can be related to a similar concept for atomic absorption or emission frequencies [3]. Since the velocity distribution of the atoms is Gaussian, there will be a range of frequencies that can be absorbed or emitted. These frequencies will therefore also be distributed according to a Gaussian function. This is the concept of Doppler broadening and can be expressed as [3]

$$g_{\mathrm{D}}(\omega) = \frac{c}{u\omega_0\sqrt{\pi}} exp\left\{ -\frac{c^2}{u^2}\left(\frac{\omega-\omega_0}{\omega_0}\right)^2 \right\}, \tag{4}$$

where c is the velocity of light. Equation 4 gives the probability distribution of absorbed or emitted frequencies around the most probable (maximum) value ω_0. The range of frequencies in the distribution function can be characterized with the full width at half maximum value as such [3]

$$\frac{\Delta\omega_{\mathrm{D}}}{\omega_0} = 2\sqrt{ln2}\frac{u}{c} \simeq 1.7\frac{u}{c}. \tag{5}$$

This equation gives the resonance broadening ω_{D} as a fraction of the resonance frequency ω_0. It also relates the mass of an atom with the Doppler broadening and provides an intuitive result; for a given temperature, u will decrease with the atomic mass and so will the broadening.

1.3.2 Scattering force

The slowing mechanism behind laser cooling is based on the scattering force F_{scatt}. It is a consequence of the excitation and dexcitation process in atoms. When a laser beam is incident on a counter-propagating beam of atoms with velocity v_{i}, as seen in figure 4, the momentum $\hbar k$ of the photons will be transferred to the atoms. This will cause the atom to change its momentum and recoil slightly. The excited state will decay after a period τ and the atom will emit radiation in a random direction. The net effect of the emitted radiation over time will cancel out and the scattering force will be equal to the rate at which the photons transfer momentum to the atom [3].

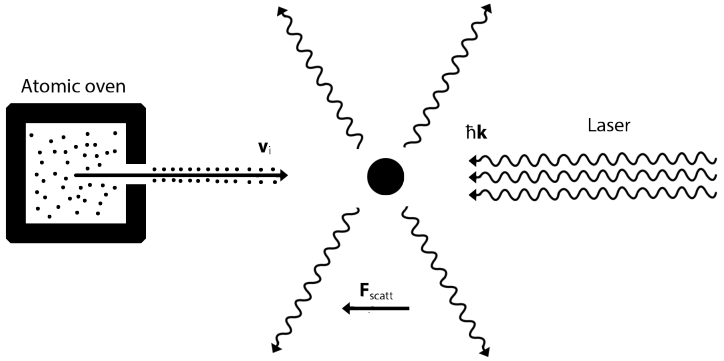

Figure 4: The figure shows the concept of the scattering force. Atoms are heated and ejected from the oven through a small nozzle as a collimated beam. The counter propagating laser excites the atoms in the beam. The atoms deexcite shortly afterwards in a random direction. The resulting force F_{scatt} then slows and starts to cool off the atoms in the beam.

The absorption rate is proportional to the radiation intensity but is also limited by the lifetime of the atomic transition. When the saturation intensity is reached the absorption rate cannot increase further. At this point F_{scatt} will be at a maximum which also gives the maximum deceleration

$$a = \frac{F_{\text{max}}}{M}, \tag{6}$$

where M is the atomic mass. Assuming a constant deceleration it is possible to rewrite this as an equation of motion [3]

$$v_{\text{i}}^2 - v_{\text{f}}^2 = 2az. \tag{7}$$

In this expression v_{i} is the initial velocity and v_{f} is the final velocity. It is also possible to calculate the distance L required to reach the final velocity [2]

$$L = \frac{v_{\text{i}}^2 - v_{\text{f}}^2}{2a}. \tag{8}$$

1.3.3 Zeeman slower

The scattering force works optimally when the laser frequency is the same as the atomic resonance frequency plus the velocity induced Doppler shift. This means that the slowing

laser needs to be detuned with respect to the atomic resonance. However, as the atoms start to slow down the Doppler shift will change. This will bring the laser out of resonance with the atom. Therefore, the laser detuning has to follow the changed Doppler shift for laser cooling to be effective. To get a continuous slowing effect it is necessary to create conditions where this is possible. This has been done in different ways historically, but here the focus will be on Zeeman slowing.

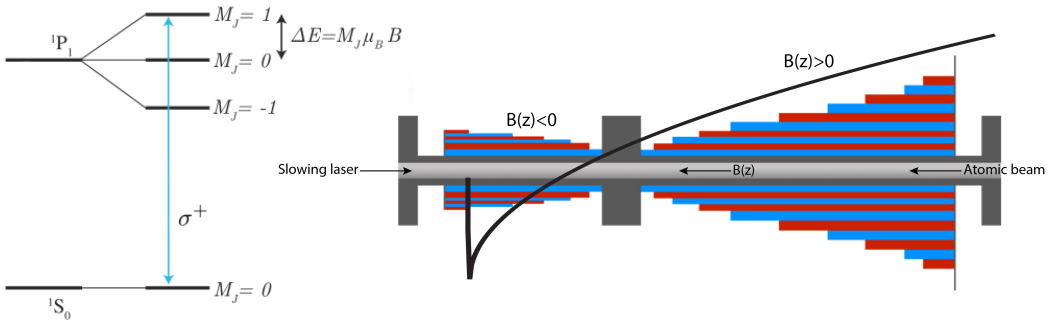

Figure 5: On the left is an atomic transition between the ground state $^1S_0$ and the states from the Zeeman effect in level $^1P_1$, chosen as an example. On the right is a schematic figure of the Zeeman slower and the slowing process. By using a σ^+-polarized and detuned laser and gradually shift the magnetic field $B(z)$ to match the state $M_J = 1$, it is possible to keep the laser in resonance with the atoms as the Doppler shift changes. Parts of the figure are adapted from [2].

The Zeeman slowing technique was developed in the 1980s as a means to deal with Doppler shift in laser cooling [6]. The idea is to use a position dependant magnetic field to change the atomic energy levels which in turn changes the resonance frequency of the atom via the Zeeman effect, see figure 5. This was originally done with a tapered coil and a similar design was used here. The following condition needs to be met in order to compensate for the Doppler shift

$$\omega_0 + \frac{\mu_\mathrm{B} B(z)}{\hbar} = \omega + kv. \tag{9}$$

The atomic resonance ω_0 and the Zeeman shift on the left hand side has to be equal to the laser frequency ω and the Doppler shift. Combining equation 7 with equation 8, this can be used to find the velocity as a function of position,

$$v = v_\mathrm{i}\left(1 - \left(1 - \frac{v_\mathrm{f}^2}{v_\mathrm{i}^2}\right)\frac{z}{L}\right)^{1/2}. \tag{10}$$

Solving for $B(z)$ by combining equations 9 and 10 yields the ideal shape of the magnetic field $B(z)$, given by

$$B(z) = B_0\left(1 - \left(1 - \frac{v_\mathrm{f}^2}{v_\mathrm{i}^2}\right)\frac{z}{L}\right)^{1/2} + B_\mathrm{bias}, \tag{11}$$

where $B_0 = \hbar k v_\mathrm{i}/\mu_\mathrm{B}$ and $B_\mathrm{bias} = \hbar(\omega - \omega_0)\mu_\mathrm{B}$. Figure 6 shows the ideal field $B(z)$ with and without a bias B_bias. One aspect of the experimental design that strongly favours using a

bias is how the laser used for Zeeman slowing is positioned. Since the atoms have to pass from the slower into the MOT without obstacles this laser is placed in the same position as the horizontal MOT laser. This means the slowing laser has to pass through the atomic cloud as it accumulates in the center of the MOT. If the frequency of the slowing laser is not carefully tuned it will cause problems when trapping atoms in the MOT. The MOT is designed so that $B_{\mathrm{MOT}} = 0$ in the center and anti-symmetric on the z-axis around this point. To keep the atoms trapped in the MOT they must have $v \sim 0$, which leads to the Doppler term $kv \sim 0$. In a slower designed without a bias the atoms reach their lowest velocity when $B(z) = 0$, which is the same condition as in the MOT. The slowing laser will therefore exert F_{scatt} on the atoms in the MOT. This will cause the otherwise symmetric trapping force in the MOT to no longer be symmetric and push the atoms out.

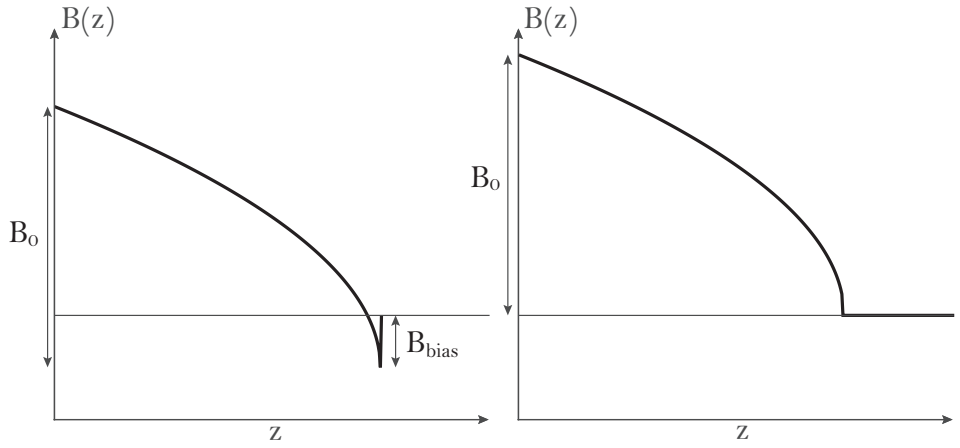

Figure 6: The figure shows the ideal shape of $B(z)$ with and without B_{bias}.

This problem can be averted by designing a Zeeman slower with $B_{\mathrm{bias}} < 0$, see figure 5. This creates a situation at the end of the slower where $B(z) < 0$, which shifts the energy level in the opposite direction. The condition for resonance becomes $\omega_0 + \mu_{\mathrm{B}} B(z)/\hbar = \omega$, since $v \sim 0$. For this to work, the slowing laser needs a fixed detuning with respect to ω_0. Bringing the field back to $B(z) = 0$ removes the Doppler shift and creates a situation where the atom passes through the detuned laser beam and no slowing occurs. This is the solution that was opted for in this setup.

1.4 Thesis outline

This thesis will investigate the Zeeman slower that is to be used for the project at SP. This piece of equipment is important for slowing and cooling the atoms before they can be trapped in the MOT. The hardware has already been manufactured so the thesis focuses on characterizing the properties of the slower. The original design of the slower was determined by parameterizing the number of coils, number of coil turns and number of layers [2]. Although the coil configuration used here closely follows the original design, some aspects differ. The original design used the magnetic field of the MOT to reduce size and energy consumption. This solution is not used here, instead a more modular and serviceable approach is used. To approximate the magnetic field profile on the left in figure 6 two coils had to be used for

the construction. Therefore, it is important to measure the magnetic field profile to make sure it is smooth and has the correct profile shape. If it is not, the performance of the clock might suffer. To avoid this situation, a manually controlled electronic control circuit was constructed. The idea behind the circuit is to individually control the current through each coil to correct the magnetic field shape of the slower.

The following sections of the thesis will explain the equipment used, the experimental setup and discuss the results. Section 2 contains details about the Hall sensor and how it was used as a Gaussmeter to measure the magnetic field profile. The section also contains the method for measuring temperature. The last part of section 2 covers the electronics and software used to construct the control circuit. Section 3 contains the results from all measurements as well as the performance of the control circuit. In section 4 the outlook and some improvements and additional features are discussed.

2 Method and experimental setup

This section describes the physical design of the slower and how some of its physical properties were measured. The Hall sensor and how it was used the magnetic field profile of the slower is described. The section also includes the control circuit design.

2.1 Hall effect sensor

2.1.1 Hall effect in semiconductors

The Hall effect is commonly used in magnetic flux measurements. The effect is a consequence of the Lorentz force $\mathbf{F}$ acting on a charge q, see figure 7. The Lorentz force can be observed in a system with both an electric field $\mathbf{E}$ and a magnetic field $\mathbf{B}$. The charge feels a force $\mathbf{F}_E = q\mathbf{E}$, due to the electric field, which causes it to move with a velocity $\mathbf{v}$. A moving charge in a magnetic field will also experience a force $\mathbf{F}_B = q\mathbf{v} \times \mathbf{B}$, orthogonal to both $\mathbf{v}$ and $\mathbf{B}$. The resulting force $\mathbf{F} = \mathbf{F}_E + \mathbf{F}_B$ can be summarized as [13]

$$\mathbf{F} = q(\mathbf{E} + \mathbf{v} \times \mathbf{B}). \tag{12}$$

The Lorentz force acting on the charges in the material will cause them to accumulate and give rise to another electric field, perpendicular to the applied field $\mathbf{E}$. It is this potential difference V_H across the material that is the Hall effect.

The expression for the Hall potential in semiconductors [15] is stated here without derivation. The formula is slightly modified to take into account the angular dependence of the magnetic field lines through the surface by including the area vector $\mathbf{A}$

$$V_H = \frac{JR_H\mathbf{B} \cdot \mathbf{A}}{w} = \frac{JR_HBA\sin\theta}{w}, \tag{13}$$

where J is the current density through the material and w is the width in the direction of the Hall potential. R_H is the Hall constant for the material and in semiconductors it is given by [15]

$$R_H = \frac{p\mu_e^2 - n\mu_h^2}{q(n\mu_e + \mu_h)}, \tag{14}$$

where p and n are the electron and hole concentrations respectively. μ_e and μ_h are the electron and hole mobility constants for the particular material used.

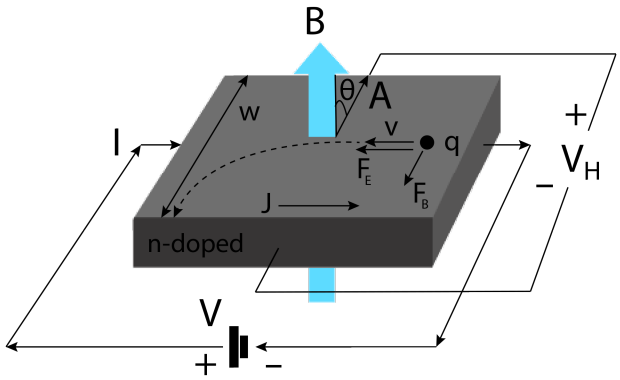

Figure 7: A voltage V applied across an n-doped semiconductor will create and electric field, which will cause a charge q to move with velocity $\mathbf{v}$. If a magnetic field $\mathbf{B}$ is also applied perpendicular to the electric field, the moving charge will feel an additional force $\mathbf{F}$ perpendicular to $\mathbf{v}$. The force will divert the motion of the charge, according to the dashed line, and create an inhomogoneous charge distribution. This gives rise to the Hall potential difference V_{H}.

2.1.2 Operating principle of the sensor

A linear semi-conductor Hall effect device [16] was used to sense the magnetic flux density inside the slower. The device consists of a Hall effect sensor connected to an integrated circuit. The device outputs an analog voltage signal proportional to the flux density through the sensor. The quiescent output V_{Q} (the output when no magnetic field is applied) is 50% of the supply voltage. The supply voltage is specified to 5 V, which would give an output of $V_{\mathrm{Q}} = 2.5$ V when no field is applied. The presence of a south-polarized magnetic field will increase the output voltage from the quiescent value towards the supply voltage. The opposite will happen in the presence of a north-polarized magnetic field. The output range is thus $0 \leq V_{\mathrm{out}} \leq 5$. The particular device used here (model A1326) has an output sensitivity of 2.5 mV/G. The magnetic sensitivity S is defined as

$$S = \frac{V_{\mathrm{out(B+)}} - V_{\mathrm{out(B-)}}}{B(+) - B(-)}. \tag{15}$$

This relationship gives the general case when comparing the output difference between two magnetic fields, $B(+)$ and $B(-)$, of opposite polarity. The baseline comparison with no applied field is Earth's magnetic field, which is < 1 G. This has not been accounted for in the measurements. The baseline was instead set to 0 G, which corresponds to $V_{\mathrm{Q}} = 2.5V$. This simplifies the above formula to

$$S = \frac{V_{\mathrm{out}} - V_{\mathrm{Q}}}{B}. \tag{16}$$

With the chosen sensitivity it is possible to measure magnetic flux densities of ± 1000 G.

2.2 Zeeman slower magnetic field measurements

The aim has mainly been to find a repeatable method without close consideration of error sources and optimization details. Also, the main purpose has been to measure the magnetic

profile produced by the coil and see how well it fits the theoretical model described by equation 11. Therefore, the measurements have not been performed with absolute values in mind. An overall view of the experiment can be found in figure 8. In all the measurements carried out the coils were connected in series and were fed a current of 0.9 A. This value was chosen because it is close to what was used in Schioppo's work [2].

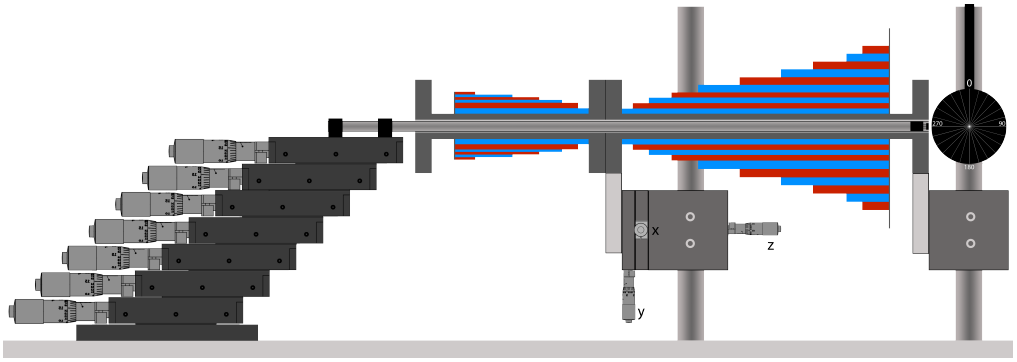

Figure 8: Above is the experimental setup that was used to measure the magnetic flux density. The slower is resting on two cradles so that it can be removed and returned to the same position. The cradles are mounted on two vertical cylinders to allow for the slower to be kept horizontal. The left cradle, on which the junction between the two slower halves is resting, can be adjusted in all directions to fine tune the position of the slower relative the sensor rod.

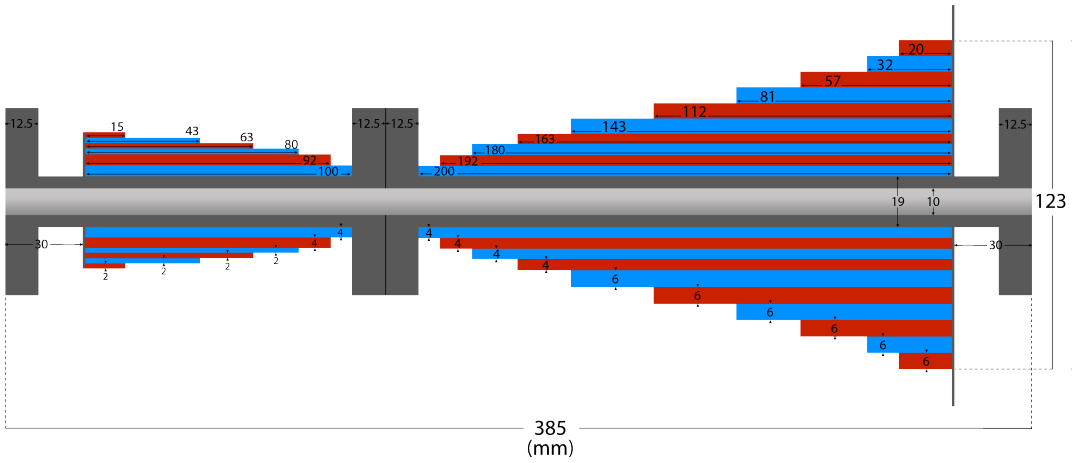

Figure 9: This figure is a cross section of the Zeeman slower with all dimensions given in mm. The right side is where the atomic oven would be mounted and where the atoms would enter. The left side is the exit and where the MOT will be connected.

2.2.1 Gaussmeter

The geometry of the slower from figure 9 requires any sensor device to be able to reach beyond a length of 385 mm. To achieve this the sensor was mounted at the end of a 450 mm long, hollow aluminium rod. The rod has an outer diameter of 8 mm, which is small enough to fit inside the slower. To allow the sensor to be switched for other sensitivities or even other sensors, a 3-pin female contact was mounted at the end of the rod.

The Hall sensor inside the electronic housing is oriented in such a way that the connector pins had to be bent 90 degrees to provide maximum flux through the sensor. This arrangement can be seen in figure 10. The coordinate axes in this figure are consistent with the axes used in figure 8.

Two of the experiments tested how the sensor device responded to varying the angles θ and α in figure 10. The angles were measured with a lens mount. A measurement series was recorded for 30, 45, 60 and 90 degrees. It was expected that given a certain point z, a uniform flux $B(z)$ and alignment of the sensor's area vector $\mathbf{A}$ along the z-axis; the flux should be invariant as α is rotated and obey equation 13 when θ is varied.

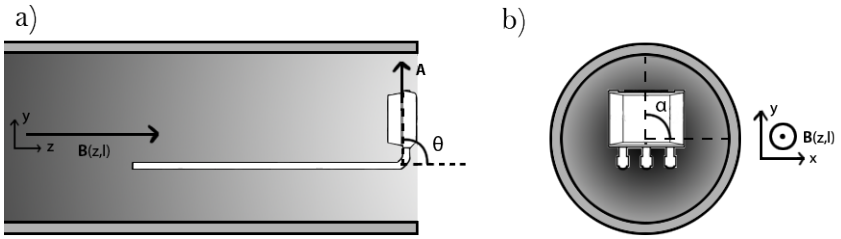

Figure 10: The figure shows how the sensor is oriented inside the probe rod. It shows the magnetic field and the sensor's area vector $\mathbf{A}$ aligned along the z-axis.

To verify if the output varied according to Equation 13, the ratio of data point $B_{i,\theta}$ and the maximum flux $B_{i,90}$ was calculated. To minimize the error in this calculation it was done for each point in the series and then averaged over the total data points N. The formula is given below

$$\sin\theta = \frac{\sum_{i=1}^{N}\left(\frac{B_{i,\theta}}{B_{i,90}}\right)}{N} \tag{17}$$

The invariance of α was tested by comparing the measurement series $B(z),\ \alpha = 0$ and $B(z),\ \alpha = 90$.

2.2.2 Moving the Hall sensor

The Gaussmeter was mounted on a stack of seven micrometer adjusters, the setup can be seen in 8. Each unit can be moved 25 mm, so the probe can be moved a total of 175 mm when all adjusters are in the most extended position. To ensure proper alignment of the probe in relation to the slower, three adjusters were mounted in an xyz arrangement, see figure 8. The probe was moved in the z-direction in steps of 10 mm and the sensor output was manually recorded. Since the slower is 385 mm the adjusters had to be reset twice to cover the entire length. The reset required the probe to be loosened from its initial position. The whole procedure can be summarized as:

1. Lock the probe in its initial position. Move all seven adjusters; the probe has now moved 175 mm.

2. Reset all adjusters and lock the probe. Move all seven adjusters once again; the probe has now moved a total of 350 mm.

3. Reset all adjusters a second time and lock the probe. Move the probe back to cover the remaining bit of the slower length.

The reset steps will likely introduce a systematic error. To counteract this, the voltage output of the sensor was used as a guide to find the last position of the probe before locking it in place. The voltmeter had a precision in the µV range and this systematic error will likely be small compared to the step size.

2.3 Zeeman slower temperature measurements

The long-term temperature stability of the coil was also of interest since the finalized clock will be designed to run continuously. A platinum wire resistance temperature detector was attached to the coil to register the temperature at the surface and was recorded with a multimeter. The resolution of the multimeter was limited to integer values. This is not a problem since it is only the final temperature that is of interest. However, to get better resolution the voltage increase across the coil was also recorded. The temperature was measured over four hours after which the temperature seemed to have stabilized.

2.4 Electronics and software

2.4.1 Arduino microcontroller

The circuit was based around the Arduino [17] hardware and programming platform. The Arduino is an open-source, rapid prototyping platform that has become popluar due to its accessibility. There are several versions available depending on the scale and project area. The Arduino boards can be programmed with a common programming language called Processing [17]. It is a simplified version of C and contains several pre-built libraries for controlling input and output. Since the platform is open-source there is a large repository of user-created code readily available.

The Zeeman slower consists of sixteen individual coils, hence sixteen analog outputs are required to control them individually. There is no single Arduino board that can handle that many outputs and therefore the choice fell on the Arduino Mega 2560 [18] to control the current through the ten coils in the first slower half. An Arduino Uno is to be used for the six coils of the second half.

2.4.2 Circuit

The overall design idea and a simplified input and output (I/O) scheme can be found in figure 11. The circuit consists of two main parts: the Arduino control unit, powered by a 5 V USB interface, and an externally powered circuit with all the coils connected in parallel. Each coil i sontrolled by an identical circuit, this unit is shown in figure 12. The circuit was designed to be able to provide $\sim 1\,\mathrm{A}$ to each coil. The full schematic consists of ten such units and can be found in appendix A. The circuit for the second half of the slower has not been designed yet.

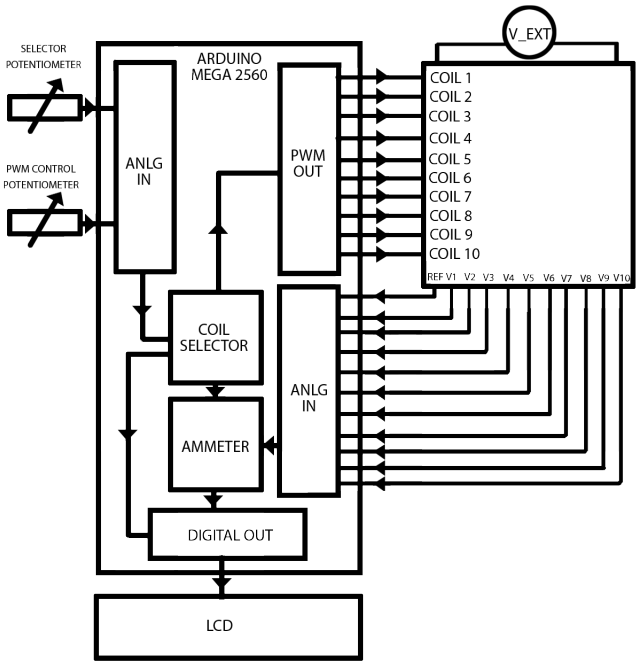

Figure 11: The figure shows a basic design outline used for the control circuit. The analog inputs are used to select a coil and control the current via code uploaded to the Arduino firmware. The analog inputs also recieve data on the voltage across each coil, which is then translated into current in the firmware. This information is presented on the LCD. The details of the external circuit can be found in appendix A.

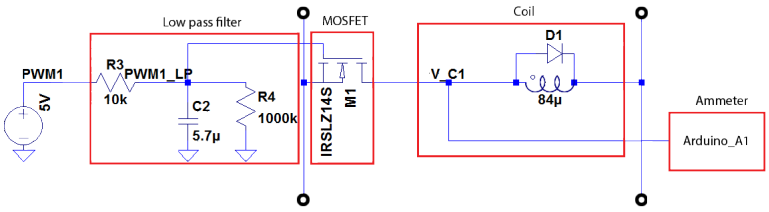

Figure 12: This circuit is used to control each coil. A 5 V PWM signal is generated to the left and passed through a low-pass filter which acts as a digital-to-analog converter. This signal then controls the gate voltage on the MOSFET transistor which in turn controls the current through the coil. To the right is the voltage input for the ammeter.

The current is controlled by a metal oxide semiconductor field effect transistors (MOSFET) [19] connected in series with each coil. They function as current valves, which in turn allows the magnetic field to be controlled. The current through each transistor is switched by a pulse width modulated (PWM) signal between 0 and 5 V from the Arduino. By switching the pulse fast enough and relying on the slow response of the system it is possible to

change the time-averaged signal by changing the pulse-on time t_{on}. The duty cycle D of a PWM signal can be used as a measure of the signal output and is defined as the ratio $D = t_{\text{on}}/T$, where T is the period of the signal.

In the case of the Arduino the modulation has a resolution of 8-bits, or equivalently, a value range between 0-255. The Arduino also allows for the PWM frequency to be changed and here it was set to 31250 Hz, which corresponds to a pulse width, or period, of $T = 32\,\mu\text{s}$. For example, if $D = 0.5$ this corresponds to a PWM value of 127 and the output pulse will be 2.5 V.

Despite this relatively high frequency, the transistor is sensitive enough that it will respond to the voltage fluctuations and cause large current variations. Therefore, a passive low-pass filter (LPF) was connected between the control signal output and the transistor input, see figure 12. The cut-off frequency for a LPF is given by $f_{\text{c}} = 1/2\pi RC$ [20], where R is the resistance and C is the capacitance connected in parallel. Choosing a high R and C will remove increasingly higher frequencies. In the limit, only the DC component will be left. Here, the filter was constructed from standard components with values; a $10\,\text{k}\Omega$ resistor, a $5.7\,\mu\text{F}$ capacitor connected to ground and a $1\,\text{M}\Omega$ resistor, also connected to ground. These values give $f_{\text{c}} \approx 3$ Hz.

The ammeter and coil selector functions shown in figure 11 were implemented in the Arduino firmware. The coil selector consists of a potentiometer which is connected to an analog input of the Arduino. This input is 10-bits, which creates a range of values between 0-1023. This range was then divided into ten parts and assigned a specific PWM output. Once a coil is selected, the value is sent to the LCD and the current can now be changed with a second potentiometer.

The ammeter takes in a reference voltage V_{EXT} from the positive rail on one of the analog inputs. Then, depending on which coil is selected, it compares this value to the voltage after the coil. Finally, the data is converted into amperes and sent to the LCD.

2.4.3 Simulation software

To further help with the design process a circuit simulation program called LTSpice was used [21]. LTSpice was mainly used to find conditions under which the current remained stable over time. Figure 21 in appendix A shows the circuit used in the simulations.

In order to perform a more accurate simulation the resistance and inductance of each coil was of interest. The series resistance was simply measured. An empirical formula derived by LA Hazeltine [22] was used to calculate the inductance of each coil. The formula is given by

$$L = \frac{0.8a^2n^2}{6a + 9b + 10c}, \tag{18}$$

where n is the number of turns, a is the distance from the center of the coil to the metal wiring midpoint, b is the length and c is the depth of the wiring layers. The calculated unit for L is µH and the input dimensions are inches. The geometry for which the formula applies is shown in figure 13. The accuracy is within 1% of the measured value for such a geometry [22]. The outer coils used here have a similar geometry but the inner coils have a geometry where $b > a$ see figure 9. For this reason it is expected that the simulation will not be perfectly accurate, but will at least provide an approximate starting point.

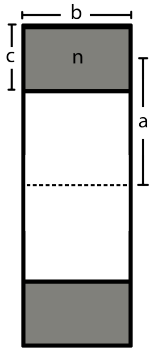

Figure 13: The image shows a cut-through view of a solenoid. The approximate geometry shown here was used to experimentally derive equation 18.

3 Results and discussion

The results given below are only relevant to the larger of the two coils in the Zeeman slower. There was not enough time to run simulations and build the circuit needed to power the second smaller coil. However, now that most of the work has been done for the large coil it should be quite easy to design a solution for the smaller one.

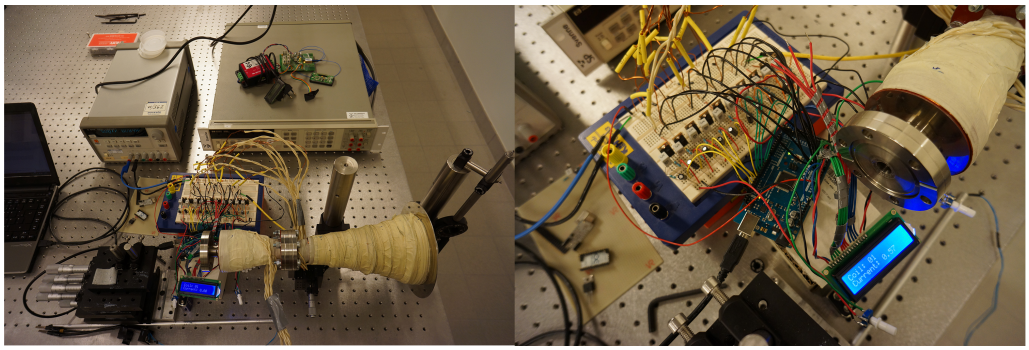

Figure 14: The figure shows a picture of the experimental setup and a close-up of the circuit.

3.1 Magnetic field and Hall sensor

Figure 15 shows how the magnetic field varies with the position in the slower for a series current of 0.9 A. The figure also shows the theoretical curve given in equation 11 and figure 6 for similar specifications. This curve is given by

$$B_{\text{ideal}}(z) = 665\left(1 - \left(1 - \frac{30^2}{500^2}\right)\frac{z}{0.3}\right)^{1/2} - 200. \tag{19}$$

Based on this curve it is possible to speculate on the performance. The most probable initial velocity was assumed to be $v_i = 500\,\text{m/s}$ for the ideal curve. The measured field is overall weaker than $B_{\text{ideal}}(z)$ and therefore it will not capture as many atoms. This can easily

be compensated by adjusting the current. It is important that the field is not too strong; otherwise the atoms will not be able to reach the MOT before they stop. The measured curve is quite smooth and even in the junction between the two coils there is almost no deviation.

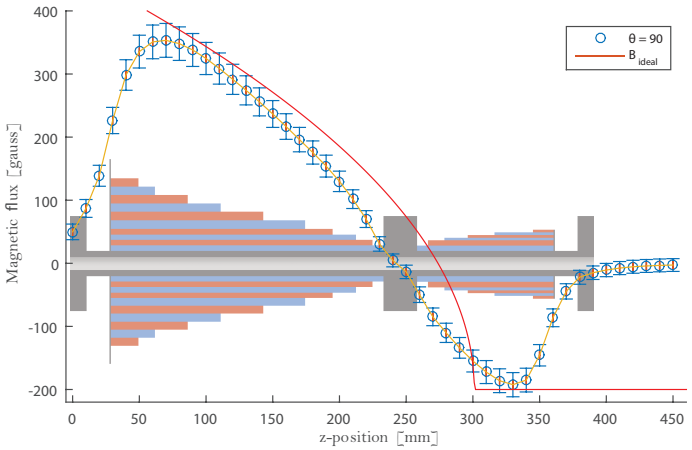

Figure 15: This figure shows the maximum flux measurement at $\theta = 90$. Both vertical and horizontal error bars are shown. It also shows the ideal curve for $B_0 = 665$ G, $v_i = 500\,\mathrm{m/s}$, $v_f = 30\,\mathrm{m/s}$, $L = 0.3\,\mathrm{m}$ and $B_{\mathrm{bias}} = -200$ G.

The smallest error in the position of the Gaussmeter is introduced by the mechanical micrometer screws. This is four orders of magnitude smaller than the step size of 10 mm and can be considered almost negligible. This can be seen in figure 15, the horizontal error bars are too small to be seen. On the other hand, a larger, systematic error is introduced each time the adjusters had to be reset and the probe rod was loosened. A ruler with millimeter precision was used to roughly align the rod. The sensor output was used to find the value of the previous data point in an attempt to minimize the error. The output was measured with a µV resolution voltmeter. This introduces, at most, an error of 1 mm in the position and ∼1 mV in the Gaussmeter output each time. Since this was done twice the error will accumulate. There are no sudden jumps in figure 15 at the points where the adjusters were reset, suggesting that the method is able to keep this error to a minimum.

There are also some error components built in to the Hall sensor that need to be considered. Drifts will occur in the voltage output and sensitivity as the ambient operating temperature increases inside the slower. The temperature of the sensor was not recorded during the measurements which limits the accuracy of the estimation. Therefore, only a worst case calculation has been made. This calculation assumes an ambient temperature of 150 °C, which is the maximum operating temperature of the sensor. At this temperature the sensitivity differs ±5% from the nominal value 2.5 mV. Also, the output voltage drift is specified to ±10 G at this temperature.

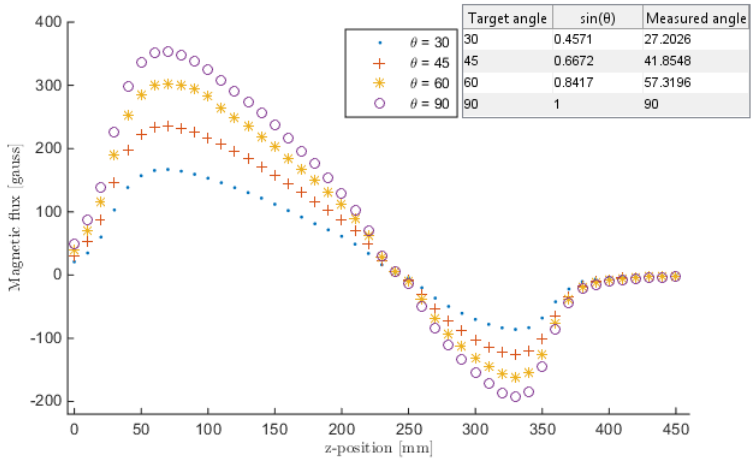

Target angle	sin(θ)	Measured angle
30	0.4571	27.2026
45	0.6672	41.8548
60	0.8417	57.3196
90	1	90

Figure 16: The figure shows how the registered magnetic field varies with the sensor angle θ. The error bars have been removed to more clearly see each data series. The hall sensor was positioned in the four different target angles and a data series was measured. The middle column in the inset table shows the result from equation 13 and the third column is the angle corresponding to each measured data series.

The results from varying θ are shown in figure 16. To calculate the average relative intensity equation 17 was used. The numerical results are shown in the inset of figure 16. From these values it was conclude that the sensor output indeed varies according to equation 13. However, the measured values are all lower than what is to be expected. It is reasonable to suspect a systematic error, but this has not been investigated further. The setup for measuring the angle is relatively crude and a systematic is not unlikely, despite this it was able to reproduce the trend expected from equation 13. The error is $\sim$ 3 degrees in all measurements.

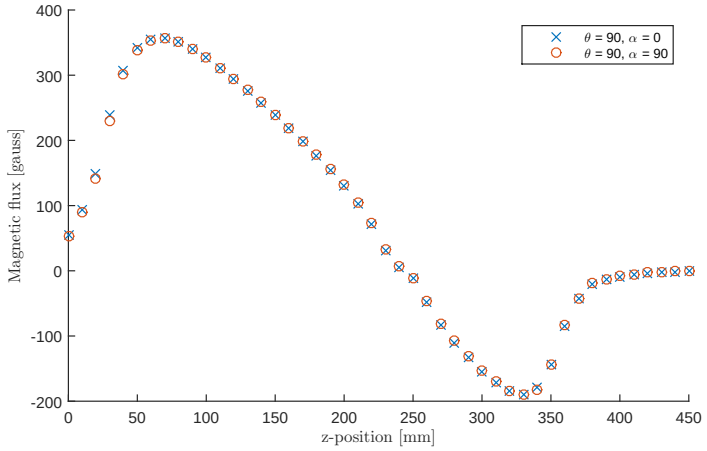

Figure 17: The figure shows how the registered magnetic field varies with the sensor angle α. The error bars have been removed to more clearly see each data series. See figure 10 for the angle definitions.

Figure 17 clearly shows how the voltage output from the Hall sensor is invariant for different angles of α. Overall, the Hall sensor performs according to theory and equation 13.

3.2 Resistance and inductance

The resistance through each coil was measured and the results are shown in table 1. These values were then used in the circuit simulation and the in the ammeter code to calculate the current. The inductance values calculated with equation 18 should not be considered accurate in absolute terms, but rather as a relative comparison to improve the simulation results. The measurements were done at room temperature and not at operating temperature.

Table 1: The table shows the measured coil resistance and calculated inductance values for the large coil. Each coil is referenced by its length.

Coil	$R[\Omega]$	L [µH]
200	1.433	84
192	1.689	135
180	1.922	191
163	2.142	240
143	3.148	292
112	2.806	310
81	2.318	276
57	1.974	219
32	1.247	115
20	0.873	64

3.3 Control circuit

The results from the simulation showed that the circuit would need a minimum of $\sim 5\,\mathrm{V}$ to operate all ten coils at $1\,\mathrm{A}$. This gives a source-to-drain voltage $V_{\mathrm{DS}} = 5\,\mathrm{V}$ over the transistors, which in turn puts a limitation on the gate voltage that can be applied in order to not exceed $1\,\mathrm{A}$ per coil. The operational range was found to be between PWM values 120 and 152 in the simulation. In the real circuit the effective PWM range was found to be between $90 \leq PWM \leq 145$. Figure 18 and 19 both show the simulation results. Figure 18 shows the time series simulation plot from LTSpice for different PWM duty cycles. Figure 19 contains a plot of the steady state current reached in the time series simulation. Figure 19 also shows how the actual current response varied in the circuit and the results are very similar to the simulation. The major difference is an offset in the PWM values. The manufacturer specifies a range of threshold voltages and there is probably a discrepancy in this value for the real and simulated component. From this plot it is clear that the current response is not linear. The current and the magnetic flux, however, are linearly related; dividing the coefficients of the two fitted curves in figure 19 gives the relation $B(I) \approx 42 \cdot I(PWM)$.

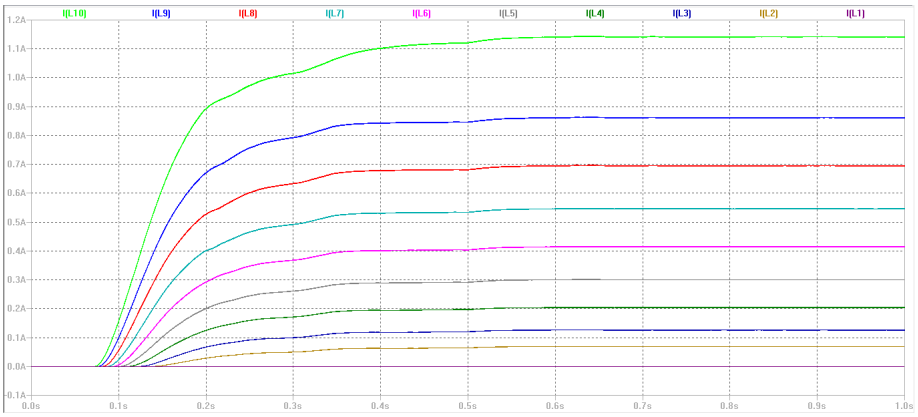

Figure 18: This figure shows the results from the circuit simulations with LTSpice. The signal is simulated over 1000 ms to reach a steady state. Each curve corresponds to the current through one of the coils for a particular PWM duty cycle $120/256 \leq D \leq 152/256$.

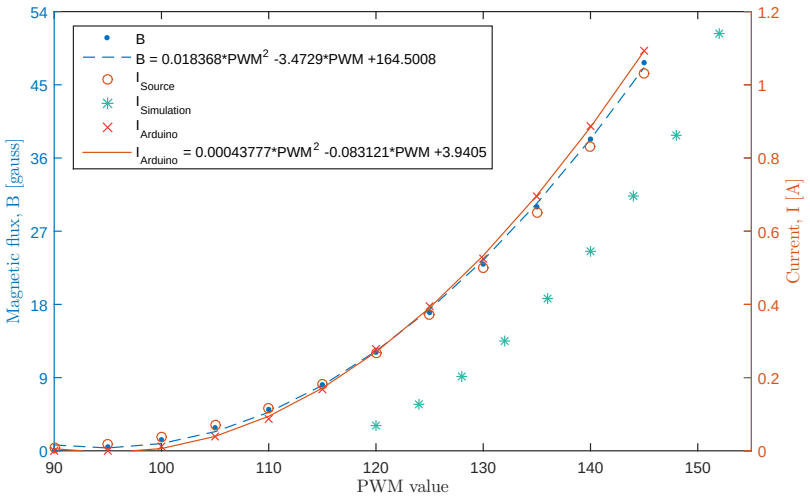

Figure 19: The figure shows how both the magnetic field varied and how the current varied as the PWM value was changed. The two fitted functions $B(PWM)$ and $I(PWM)$ only differ by a factor of ~ 42. The simulated results are offset compared to the real values, likely due to a difference in transistor threshold voltages. The current readings from both the source and the Arduino have been plotted to show their similarities.

Furthermore, because of the chosen parameters $V_{\text{EXT}} = 5\,\text{V}$ and $I_{\text{coil}} \leq 1\,\text{A}$ the transistor is operating in a non-linear regime. Therefore the resolution R will vary throughout the operational range and it is interesting to see what the lowest resolution is. R is taken to be the change in output response for an increase in the PWM value. The derivative of the fitted function $B(PWM)$ (dashed line) in figure 19 describes how the resolution changes with an increase of the PWM value. This function is given by

$$R(PWM) = \frac{dB}{dPWM} = 0.036736PWM - 3.4729. \tag{20}$$

In the operational range this means $0.2\ \text{G} < R < 2\ \text{G}$. The response could be made more linear, to some extent, by adjusting the range of PWM values the potentiometer controls. The first points between 90-115 take up ~ 50 % of the operational PWM range but only contribute ~ 20 % of the flux output range. By setting the starting value to 115 the function would become more linear.

The discrepancy between I_{Source} and I_{Arduino} in figure 19 could be explained by not having taken the internal transistor resistance into account. The ammeter in the Arduino calculates the current based on voltage and is therefore reliant on accurate resistance input. However, it has to be investigated further to be certain.

Another consideration is the ammeter response time and accuracy. Since it is time averaged there is a trade-off between responsiveness and accuracy. It is designed to take one sample each time the Arduino loops the code and then displays the average of 1000 samples. This gives an update rate of about $\sim 1\,\text{s}$ and precision on the mA level. However, if it is to be used with the potentiometer to vary the current, the responsiveness needs to be improved. An average of 150 samples was tested which was quite responsive but in turn it

worsened the precision by roughly two orders of magnitude. The code for the control circuit can be found in B.

So far the circuit is a prototype and will not be able to sustain long term operation. This is mainly because the transistors get very hot and a cooling solution would be needed to provide long term stability. The single transistor that was tested in figure 19 was however cooled between two aluminium slabs to make sure no current drifts were present. Another factor that limited the testing was the voltage source used. It could only provide a maximum of 6 V and 5 A, which is not enough to provide 1 A through all ten coils.

3.4 Temperature

The temperature data series shown in figure 20 has a very low resolution, which is why the voltage increase across the coil is also shown. This data series has a much higher resolution. The trend is clear from both measurements and the temperature reaches an equilibrium state with the room temperature at around 35 °C.

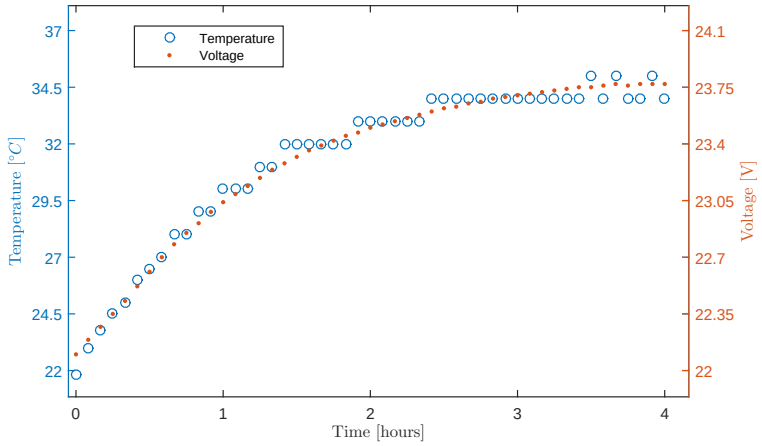

Figure 20: Both the temperature and the voltage are shown in the figure as a function of time.

In figure 20 it is clear that the surface temperature stays below 40 °C, which is low enough to not require cooling. This is taken as an indicator that the ambient temperature inside the slower is well below the maximum rating of the sensor. Therefore it is safe to assume that the actual error is smaller than what the error bars show.

4 Conclusion and outlook

There are several areas of this thesis project that are not yet completely finished or that could be improved. The first issue would be to redo the experiments with better preparations to better quantify the errors. This could be achieved by motorizing the Hall sensor movement and also by recording the sensor temperature.

The measurements of the magnetic profile revealed that the control circuit will likely not be necessary for the final clock to work well. The measured profile is smooth and matches

the ideal profile enough that operating the slower with a series current is good enough. Furthermore, the power drain would increase by a factor of around five if the control circuit is used which is also a consideration. However, the circuit could be used in other applications where current switching is needed.

Before this can be realized, there are a few things that need to be addressed. The code for the control circuit is missing a few features to make it fully functional, mainly when controlling it with the potentiometers. When selecting a coil the current through it will reset to whatever value the Arduino is currently reading from the gain potentiometer. Because of this the circuit does not save a previously selected value. The circuit would also have to be tested with a more powerful voltage source to evaluate performance under operational conditions. It would also have to be soldered or etched onto a proper circuit board and mounted in a case with sufficient cooling.

The inductance calculations could also have been improved. The calculation is based on the geometry of a radio coil which did not fit all coils in the slower. It would have been interesting to make a better model and perhaps simulate it on a computer.

A External circuit

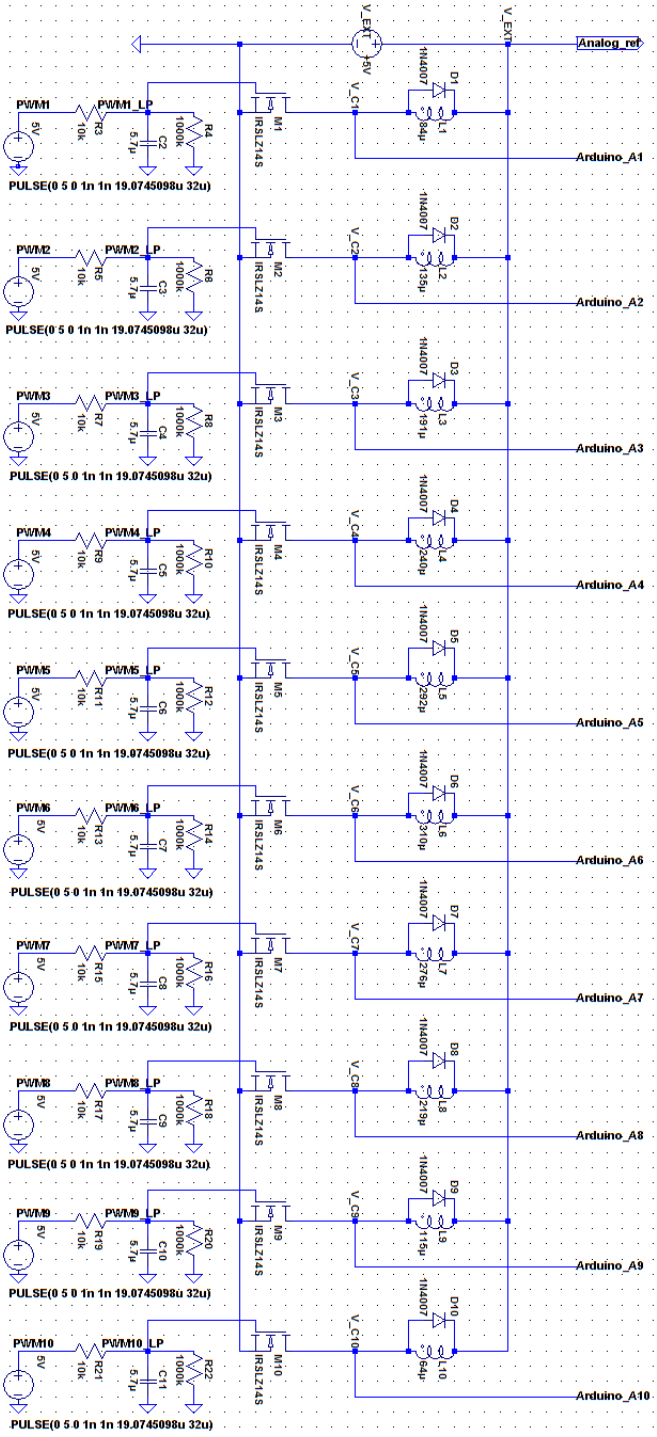

Figure 21: The figure shows the setup used to simulate the external circuit. The control signal is fed from the left and passes through the low-pass filter before it reaches the transistor gate.

B Control circuit code

```
// Includes the LCD library with pre-defined functions for input and
    output
#include <LiquidCrystal.h>
LiquidCrystal lcd(52, 53, 28, 26, 24, 22); // specifies which digital
    ouputs that are connected to the LCD

// These are the variables used to control the PWM output from the serial
    interface
char datain[7];
int index;
int seconds = 0;
int coilVal;
char digit[2];
String coil;

// These are the variables used to construct the AMMETER
double ref;
double in;
double vout;
double iout;
double rms;
int c1;
int c2;

// Variables for the COIL SELECTOR
int sel_input;
int sel_coil;
double resistance;

// Variables for the CURRENT CONTROL. 'pwm_0' sets the PWM output value
    that corresponds to 0
// current through a coil. 'pwm_range' gives the operational PWM range for
     the MOSFET. PWM(90)=0,
// PWM(140)=1A.
float current_in;
int pwm_0 = 90;
int pwm_range = 50;
int pwm_out = 0;

void setup() {
  // Starts the serial communication with the arduino,
  // baud rate is set to 115200 bits/s
  Serial.begin(115200);
  lcd.begin(16, 2);
  lcd.print("Coil:");
  lcd.setCursor(0,1);
  lcd.print("I:");
  lcd.setCursor(8,1);
  lcd.print("V:");
  //This changes the PWM output frequency from 490 Hz to 31250 Hz.
  TCCR1B = TCCR1B & 0b11111000 | 0x01;
  TCCR2B = TCCR2B & 0b11111000 | 0x01;
  TCCR3B = TCCR3B & 0b11111000 | 0x01;
  TCCR4B = TCCR4B & 0b11111000 | 0x01;
}

// Starts a loop that listens for commands from the
// serial monitor and analog inputs. The control signal can be
```

```
// controlled by sending for instance '1:0', which sets the current
    through
// coil 1 to zero. Sending 1:255 sets it to max.
// This can be summarized as 'coil:PWM:value'. There is also a command '
    all:PWM value'
// Which changes the control signal on all coilds. It can also be
    controlled with the
// potentiometer.
void loop() {

  // [POTENTIOMETER] COIL SELECTOR. The code below is deisgned to check
      which coil is
  // selected with the potentiometer. The 10-bit range is divided into 10
      parts and each subrange
  // will select a coil by changing 'sel_coil'. The ammeter below
      calculates the current based on the
  // input voltage with Ohms law, I=U/R. The inverse 1/R has been
      calculated to avoid division operations
  // and save processing power.
  sel_input = analogRead(14);
  if((sel_input >= 0) && (sel_input <= 101)){
    sel_coil = 1;
    resistance = 0.6978;    // This is the inverse of the resistance, 1/R.
  }
  if ((sel_input >= 102) && (sel_input <= 203)){
    sel_coil = 2;
    resistance = 0.5921;
  }
  if ((sel_input >= 204) && (sel_input <= 305)){
    sel_coil = 3;
    resistance = 0.5203;
  }
  if ((sel_input >= 306) && (sel_input <= 407)){
    sel_coil = 4;
    resistance = 0.4669;
  }
  if ((sel_input >= 408) && (sel_input <= 509)){
    sel_coil = 5;
    resistance = 0.3177;
  }
  if ((sel_input >= 510) && (sel_input <= 611)){
    sel_coil = 6;
    resistance = 0.3564;
  }
  if ((sel_input >= 612) && (sel_input <= 713)){
    sel_coil = 7;
    resistance = 0.4314;
  }
  if ((sel_input >= 714) && (sel_input <= 815)){
    sel_coil = 8;
    resistance = 0.5066;
  }
  if ((sel_input >= 816) && (sel_input <= 917)){
    sel_coil = 9;
    resistance = 0.8019;
  }
  if ((sel_input >= 918) && (sel_input <= 1023)){
    sel_coil = 10;
    resistance = 1.1453;
  }
```

```
  if(sel_coil != 10) {
    lcd.setCursor(6,0);
    lcd.print(0);
    lcd.setCursor(7,0);
    lcd.print(sel_coil);
  }
  else {
    lcd.setCursor(6,0);
    lcd.print(sel_coil);
  }

  // [POTENTIOMETER] CURRENT CONTROL. This section controls how much
      current goes through each coil.
  // 'current_in' gets the the potentiometer value from analog input 13
      and calculates the input
  // as a fraction of the maximum, 1024. 'pwm_out' calculates the PWM
      output based on the zero
  // current point pwm_0 and adds a fraction of the pwm_range based on the
       potentiometer input.
  // In other words, it translates the potentiometer input fraction to a
      PWM output fraction in
  // the operational range of the MOSFET.
//  if  (sel_coil == 1) {
//    current_in = analogRead(13)*0.0009765625;  //0.0009765625=1/1024, C
    requires less CPU power to multiply.
//    pwm_out = pwm_0 + (pwm_range*current_in);
//    analogWrite(2, pwm_out);
//  }
//  if  (sel_coil == 2) {
//    current_in = analogRead(13)*0.0009765625;
//    pwm_out = pwm_0 + (pwm_range*current_in);
//    analogWrite(3, pwm_out);
//  }
//  if  (sel_coil == 3) {
//    current_in = analogRead(13)*0.0009765625;
//    pwm_out = pwm_0 + (pwm_range*current_in);
//    analogWrite(5, pwm_out);
//  }
//  if  (sel_coil == 4) {
//    current_in = analogRead(13)*0.0009765625;
//    pwm_out = pwm_0 + (pwm_range*current_in);
//    analogWrite(6, pwm_out);
//  }
//  if  (sel_coil == 5) {
//    current_in = analogRead(13)*0.0009765625;
//    pwm_out = pwm_0 + (pwm_range*current_in);
//    analogWrite(7, pwm_out);
//  }
//  if  (sel_coil == 6) {
//    current_in = analogRead(13)*0.0009765625;
//    pwm_out = pwm_0 + (pwm_range*current_in);
//    analogWrite(8, pwm_out);
//  }
//  if  (sel_coil == 7) {
//    current_in = analogRead(13)*0.0009765625;
//    pwm_out = pwm_0 + (pwm_range*current_in);
//    analogWrite(9, pwm_out);
//  }
//  if  (sel_coil == 8) {
//    current_in = analogRead(13)*0.0009765625;
```

```
//    pwm_out = pwm_0 + (pwm_range*current_in);
//    analogWrite(10, pwm_out);
//  }
//  if  (sel_coil == 9) {
//    current_in = analogRead(13)*0.0009765625;
//    pwm_out = pwm_0 + (pwm_range*current_in);
//    analogWrite(11, pwm_out);
//  }
//  if  (sel_coil == 10) {
//    current_in = analogRead(13)*0.0009765625;
//    int pwm_out = pwm_0 + (pwm_range*current_in);
//    analogWrite(12, pwm_out);
//  }

  // [SERIAL] The while loop goes through the serial buffer input,
  // for instance for the input '1:123', and saves each character in a
      char array
  index = 0;
  while(Serial.available() > 0 && index < 7) {
    char aChar = Serial.read();
    datain[index] = aChar;
    index++;
    datain[index] = '\0';  // Keep the string NULL terminated because of
        ASCII formatting
  }

  // Converts the char array to a string to check for coil
  // destination
  String coil = datain;

  // The following 11 if statements checks where to send the serial input
      PWM value.
  if (coil.startsWith("1:")) {
    Serial.println(datain);
    digit[0] = datain[2];
    digit[1] = datain[3];
    digit[2] = datain[4];
    coilVal = atoi(digit);
    analogWrite(2, coilVal);
  }

  if (coil.startsWith("2:")) {
    Serial.println(datain);
    digit[0] = datain[2];
    digit[1] = datain[3];
    digit[2] = datain[4];
    coilVal = atoi(digit);
    analogWrite(3, coilVal);
  }

  if (coil.startsWith("3:")) {
    Serial.println(datain);
    digit[0] = datain[2];
    digit[1] = datain[3];
    digit[2] = datain[4];
    coilVal = atoi(digit);
    analogWrite(5, coilVal);
  }

  if (coil.startsWith("4:")) {
```

```
    Serial.println(datain);
    digit[0] = datain[2];
    digit[1] = datain[3];
    digit[2] = datain[4];
    coilVal = atoi(digit);
    analogWrite(6, coilVal);
  }

  if (coil.startsWith("5:")) {
    Serial.println(datain);
    digit[0] = datain[2];
    digit[1] = datain[3];
    digit[2] = datain[4];
    coilVal = atoi(digit);
    analogWrite(7, coilVal);
  }

  if (coil.startsWith("6:")) {
    Serial.println(datain);
    digit[0] = datain[2];
    digit[1] = datain[3];
    digit[2] = datain[4];
    coilVal = atoi(digit);
    analogWrite(8, coilVal);
  }

  if (coil.startsWith("7:")) {
    Serial.println(datain);
    digit[0] = datain[2];
    digit[1] = datain[3];
    digit[2] = datain[4];
    coilVal = atoi(digit);
    analogWrite(9, coilVal);
  }

  if (coil.startsWith("8:")) {
    Serial.println(datain);
    digit[0] = datain[2];
    digit[1] = datain[3];
    digit[2] = datain[4];
    coilVal = atoi(digit);
    analogWrite(10, coilVal);
  }

  if (coil.startsWith("9:")) {
    Serial.println(datain);
    digit[0] = datain[2];
    digit[1] = datain[3];
    digit[2] = datain[4];
    coilVal = atoi(digit);
    analogWrite(11, coilVal);
  }

  if (coil.startsWith("10:")) {
    Serial.println(datain);
    digit[0] = datain[3];
    digit[1] = datain[4];
    digit[2] = datain[5];
    coilVal = atoi(digit);
    analogWrite(12, coilVal);
```

```
  }

  if (coil.startsWith("all:")) {
    Serial.println(datain);
    digit[0] = datain[4];
    digit[1] = datain[5];
    digit[2] = datain[6];
    coilVal = atoi(digit);
    analogWrite(2, coilVal);
    delay(10);
    analogWrite(3, coilVal);
    delay(10);
    analogWrite(5, coilVal);
    delay(10);
    analogWrite(6, coilVal);
    delay(10);
    analogWrite(7, coilVal);
    delay(10);
    analogWrite(8, coilVal);
    delay(10);
    analogWrite(9, coilVal);
    delay(10);
    analogWrite(10, coilVal);
    delay(10);
    analogWrite(11, coilVal);
    delay(10);
    analogWrite(12, coilVal);
  }

  // Clears the String and char variables for the next
  // serial input command.
  coil = 0;
  for( int i = 0; i < 7; i++ ) {
    datain[i] = '0';
  }

  // AMMETER, calibrated for 2V. The ammeter is time-averaged to get a
      better value.
  // 'ref' stores all the reference voltage readings. 'in' stores the all
      the voltage readings for
  // the selected coil. Because of some weird compilation
  // error the counter had to be divided on two variables c1 and c2.
  ref += analogRead(0);
//  delayMicroseconds(20);
  in += analogRead(sel_coil);

  c1 += 1;
  c2 = 0;
  if (c1 == 1000) {
    ref = ref*0.001;    // 0.001 is 1/1000. ref is averaged over 1000
        readings.
    in = in*0.001;      // same as above
    vout = (5*ref*0.0009765625)*((ref-in)/ref);// the maximum allowed
        reading is 5V.
    iout = vout*resistance;
    rms = sqrt(iout);
    Serial.println(iout,3);  // prints the current to the serial monitor
    lcd.setCursor(2,1);
    lcd.print(iout,3);      // prints the current to the LCD monitor.
    lcd.setCursor(10,1);
```

```
    lcd.print(vout,3);      // prints the voltage across the coil to LCD.
    ref = 0;
    in = 0;
    vout = 0;
    iout = 0;
    c2 = 1;
  }
  if (c2 == 1) {
    c1 = 0;
  }

}
```

References

[1] http://www.bipm.org/. The International System of Units (SI) (Bureau International des Poids et Mesure).

[2] Schioppo M. Development of a Transportable Strontium Optical Clock. *Doctoral Dissertation University of Florence, Department of Physics and Astronomy*, 2010.

[3] C. J. Foot. Atomic Physics. Oxford Master Series in Atomic, Optical and Laser Physics, 2013.

[4] Theodor W Hänsch. Nobel lecture: Passion for precision. *Reviews of Modern Physics*, 78(4):1297, 2006.

[5] Steven Chu. The manipulation of neutral particles. *Reviews of Modern Physics*, 70(3):685–706, 1998.

[6] William D Phillips. Laser cooling and trapping of neutral atoms. *Reviews of Modern Physics*, 70(3), 1998.

[7] Claude N Cohen-Tannoudji. Manipulating atoms with photons. *Reviews of Modern Physics*, 70(3), 1998.

[8] Wolfgang Ketterle. Nobel lecture: When atoms behave as waves: Bose-Einstein condensation and the atom laser. *Reviews of Modern Physics*, 74(4):1131–1151, 2002.

[9] Eric A Cornell and Carl E Wieman. Nobel Lecture: Bose-Einstein condensation in a dilute gas, the first 70 years and some recent experiments. *Reviews of Modern Physics*, 74(3):875, 2002.

[10] David J Wineland. Nobel Lecture: Superposition, entanglement, and raising Schrödinger's cat. *Reviews of Modern Physics*, 85(3):1103, 2013.

[11] Masao Takamoto, Feng-Lei Hong, Ryoichi Higashi, and Hidetoshi Katori. An optical lattice clock. *Nature*, 435(7040):321–324, 2005.

[12] William J Riley. Handbook of frequency stability analysis. 2008.

[13] Hugh D Young and Roger A Freedman. Sears and Zemansky's University Physics 13th edition. 2011.

[14] Th Udem, R Holzwarth, and Theodor W Hänsch. Optical frequency metrology. *Nature*, 416(6877):233–237, 2002.

[15] Safa Kasap. Hall effect in semiconductors. *University of Saskatchewan*, 1990.

[16] Datasheet, Linear Hall Effect Sensor ICs with Analog Output, A1324-5-6. publication A1324DS rev. 4. *Allegro Microsystems, Worcester, Massachusetts*, 2013.

[17] Massimo Banzi. Getting Started with Arduino. 2009.

[18] Datasheet, ATmega2560 Microcontroller Data. publication 2549Q-AVR-02/14. *Atmel Corporation, San Jose, CA*, 2014.

[19] Datasheet, Power MOSFET IRLZ14. publication 91325 S11-0519-Rev. C and 71195 Rev. 01-Nov-10. *Vishay Siliconix*, 2011.

[20] Hans Lundqvist. Analog kretsteknik. *Liber Utbildning*, 1992.

[21] Linear Technology. http://www.linear.com/designtools/software/. Retrieved: 2014-11-25.

[22] Harold A Wheeler. Simple inductance formulas for radio coils. *Radio Engineers, Proceedings of the Institute of*, 16(10):1398–1400, 1928.